REVISED DIAGNOSTIC DIAGRAMS FOR PLANETARY NEBULAE

H. Riesgo and J. A. López

Instituto de Astronomía

Universidad Nacional Autónoma de México, Ensenada, B. C., México

RESUMEN

Se presentan diagramas de diagnóstico de densidad electrónica-excitación para una muestra de 613 nebulosas planetarias. En base a esta extensa muestra se definen nuevos límites estadísticos para la distribución de nebulosas planetarias en los planos log [Hα/[S II]] versus log [Hα/[N II]], log [Hα/[S II]] versus [S II] $\lambda\lambda$6717/6731 y log [Hα/[N II]] verus [S II] $\lambda\lambda$6717/6731. Los diagramas proveen una buena representación de los intervalos de condiciones físicas, indicado por estos cocientes de líneas de emisión, presentes en nebulosas planetarias en diferentes estados de evolución.

ABSTRACT

Diagnostic diagrams of electron density-excitation for a sample of 613 planetary nebulae are presented. The present extensive sample allows the definition of new statistical limits for the distribution of planetary nebulae in the log [Hα/[S II]] versus log [Hα/[N II]], log [Hα/[S II]] versus [S II] $\lambda\lambda$6717/6731, and log [Hα/[N II]] versus [S II] $\lambda\lambda$6717/6731 planes. The diagrams provide a good representation of the ranges of physical conditions, indicated by these emission line ratios, present in planetary nebulae during different evolutionary stages.

Key Words: **ISM: PLANETARY NEBULAE**

1. INTRODUCTION

Plots of emission line ratios provide useful diagnostics of the physical conditions and identification of classes of ionized gaseous nebulae. Electron density-excitation diagrams were introduced by Sabbadin, Minello, & Bianchini (1977), SMB77 hereafter, with the specific purpose of clarifying the nature of the nebula S 176. These diagrams compare the relative line intensities of the Hα/[N II], [S II] $\lambda\lambda$6717/6731, and Hα/[S II] ratios observed in supernova remnants, planetary nebulae (PNe) and H II regions. These nebulae are expected to occupy distinct regions in the diagrams as a consequence of the different physical processes operating within them. For example, supernova remnants are mainly shock excited nebulae, where low Hα/[N II] and Hα/[S II] ratios are expected across a range of electron densities. H II regions are photoionized nebulae that show a restricted range of excitation conditions and electron densities in their generally diluted environments. Meanwhile, planetary nebulae show a wide range of excitation conditions and electron densities

depending upon their evolutionary stage, the possible presence of collimated outflows and shocks and the progenitor mass, that may influence the observed Hα/[N II] ratio.

Recently, Phillips (2004) has discussed the distribution and significance of other relevant emission line ratios in PNe. Emission line ratio plots have also been used to distinguish planetary from symbiotic nebulae (e.g., Gutiérrez Moreno, Moreno, & Cortéz 1995). The SMB77 diagrams have proven to be a useful diagnostic tool for PNe and have been used widely in a number of works (e.g., Barral et al. 1982; López & Meaburn 1983; García Lario et al. 1991; Tajitsu et al. 1999). In the case of PNe the data in these diagrams often fall outside the original boundaries fit by SMB77, most likley as a consquence of the limited sample available then to set the diagram limits. The information used originally by SMB77 to define the parameter space for the PNe was obtained from the limited compilation made by Kaler (1976), where relative emission line intensities observed in planetary and diffuse nebulae are listed from differ-

ent sources. The estimated available number of PNe with the required information in that catalogue is of only about 40 objects. The information for H II regions in SMB77 was also obtained from that same source, whereas the data for Supernova remnants was taken from Daltabuit, D'Odorico, & Sabbadin (1976), Sabbadin & D'Odorico (1976), and Dopita (1976).

Here we have taken advantage of line intensities listed in the Strasbourg Catalogue of Galactic Planetary Nebulae, part II, SCGPN II hereafter, (Acker et al. 1992) to explore the empirical location of PNe in the SMB77 diagrams, but now based upon a much larger and homogeneous sample.

2. THE SAMPLE

In order to update the parameter intervals of the log $[H\alpha/[N\,II]]$, $[S\,II]$ $\lambda\lambda6717/6731$, and log $[H\alpha/[S\,II]]$ line ratios for PNe, we have compiled a database with 613 objects from the SCGPN II that provide the line intensities required in the diagrams.

The $H\alpha/[N\,II]$ ratio involves both $[N\,II]$ lines, namely $\lambda6548$ and $\lambda6584$, whereas the SCGPN II provides only data for the stronger $\lambda6584$ line. We have included the contribution from the $\lambda6548$ line by assuming a typical ratio $\lambda6584/\lambda6548 = 2.94$.

Figures 1, 2, and 3 show the distribution of the present dataset compared with the original zones for PNe, H II Regions and SNR as proposed by SMB77. The present sample requires an expansion of the original axes limits. Fig. 1 shows the log $[H\alpha/[S\,II]]$ versus log $[H\alpha/[N\,II]]$ intensity ratios; Fig. 2 the log $[H\alpha/[S\,II]]$ versus $[S\,II]$ $\lambda\lambda6717/6731$ ratios, and Fig. 3 the log $[H\alpha/[N\,II]]$ versus $[S\,II]$ $\lambda\lambda6717/6731$ ratios. In Figs. 2 and 3 we have added dashed horizontal lines that indicate the range for which the $[S\,II]$ intensity ratio is a reliable indicator of the electron density (Osterbrok 1974). The corresponding electron density scales are included on the right axes of these figures. Fig. 1 and Figure 4 contain the 613 objects in our sample; Fig. 2 and 3, and Figure 5 and Figure 6, that involve the $[S\,II]$ $\lambda\lambda6717/6731$ ratio contain only 550 objects for there were 52 objects with only one $[S\,II]$ line listed in the SCGPN II which precluded obtaining the $[S\,II]$ line ratio. Likewise, eleven additional objects were also discarded in those diagrams for having an unlikely large $[S\,II]$ $\lambda\lambda6717/6731 > 2$.

3. DISCUSSION

It is clear from Figs. 1 through 3 that the limits and zones defined for PNe in the original sample used by SMB77 fall short of covering substantial data regions in these diagrams. The present extended
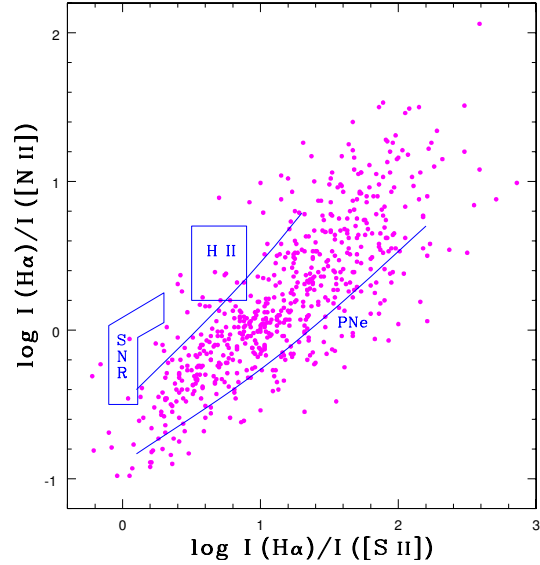

Fig. 1. The database used in this work is plotted in the log $[H\alpha/[S\,II]]$ versus log $[H\alpha/[N\,II]]$ plane. The original zones for SNR, H II regions and PNe proposed by SMB77 are indicated.
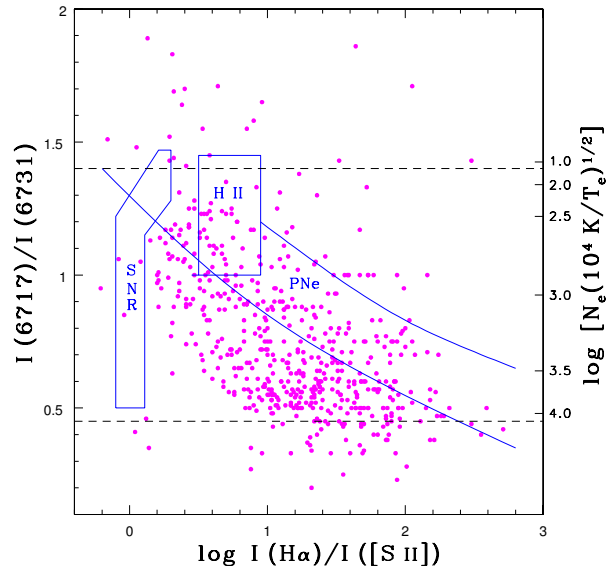

Fig. 2. As in Figure 1, but for the log $[H\alpha/[S\,II]]$ versus $[S\,II]$ $\lambda\lambda6717/6731$ plane. The horizontal dashed lines indicate the range of values for which the $[S\,II]$ $\lambda\lambda6717/6731$ ratio is a valid indicator of the electron density.

sample from the SCGPN II expands the previous location of PNe in the diagrams, providing a more accurate representation of their zones of influence.
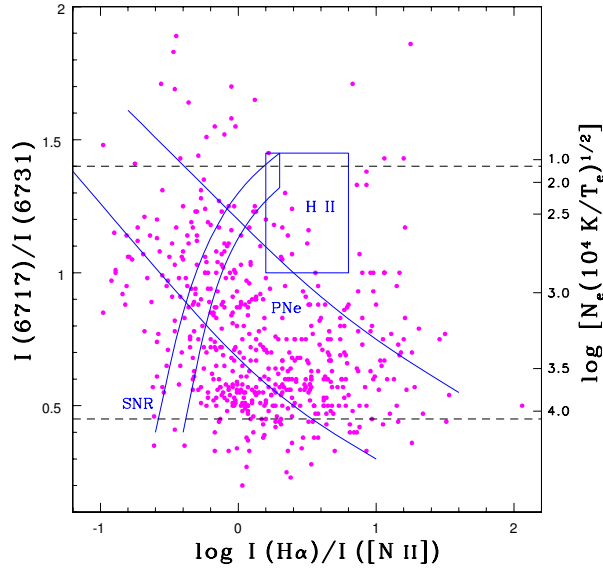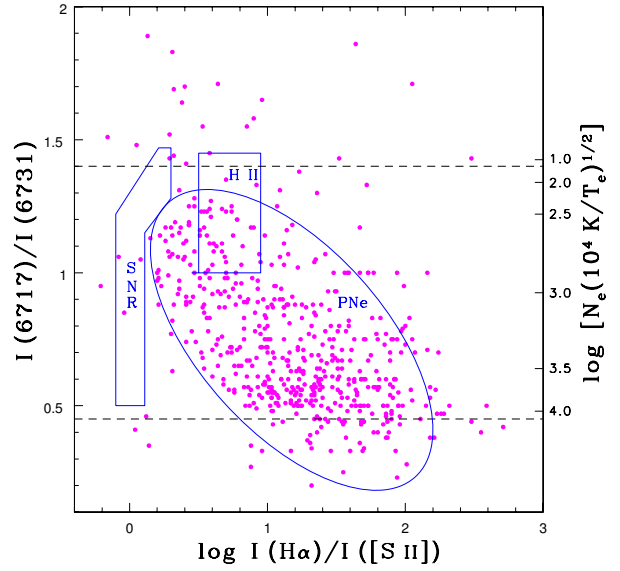
Fig. 3. As in Figure 1, but for the log [Hα/[N II]] versus [S II] λλ6717/6731 plane. The horizontal dashed lines indicate the range of values for which the [S II] λλ6717/6731 ratio is a valid indicator of the electron density.

Fig. 5. As in Figure 4, but for the log [Hα/[S II]] versus [S II] λλ6717/6731 plane. The correlation coefficient is −0.58.
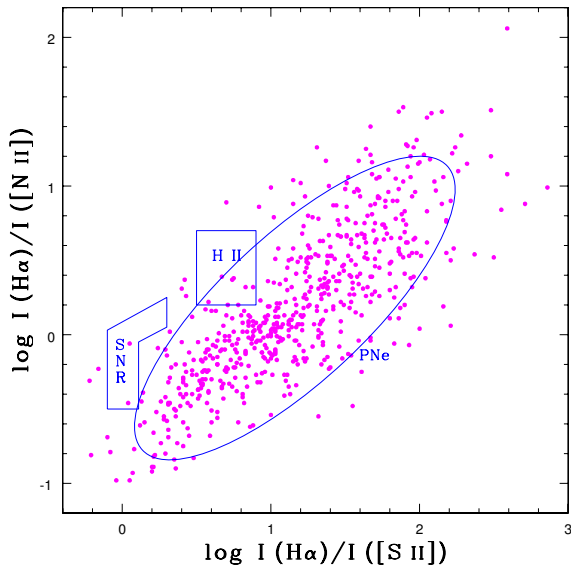

Fig. 4. Diagnostic diagram for the log [Hα/[S II]] intensity ratio versus log [Hα/[N II]] ratio with the new limits defined by a density ellipse of probability 0.85. The correlation coefficient is 0.79.
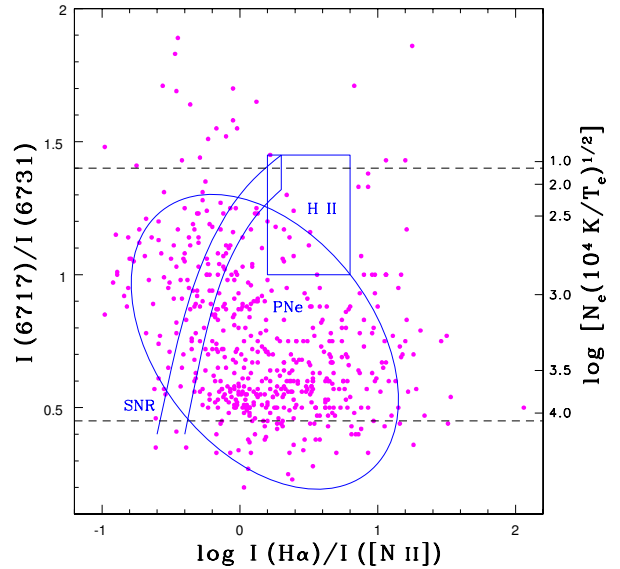
Fig. 6. As in Figure 4, but for the log [Hα/[N II]] versus [S II] λλ6717/6731 plane. The correlation coefficent is −0.37.

New statistical limits therefore have now been set to represent the location of PNe in the SMB77 diagrams by means of density ellipsoid probabilities. Figs. 4, 5, and 6 show the new zones defined

by ellipses of probablity 0.85 for the corresponding emission line ratios for PNe. The ellipse in the diagrams represents both the density contour and confidence region of finding an object within this zone

related to the scatter of the points in the diagrams and this scatter is a combination of a real dispersion due to different physical conditions, as those expected from different evolutionary stages of a planetary nebula, different conditions within a nebula (e.g., core, rim or halo) and, in some cases, also probable observational uncertainties or measuring errors from the spectroscopic SCGPN II survey. Phillips (2004) has discussed a number of factors that potentially affect such samples, such as the aperture (slit) size and its location over the nebula.

The samples for each diagram follow the trends apparent in the original SMB77 diagrams, though now they cover zones where the concentration and correlation of the line ratios provide a much closer representation of the true location of PNe in these diagnostic diagrams. For example, the ellipses in Figs. 5 and 6 show a clear tendency towards larger electron density values as compared to the corresponding original areas indicated in Figs. 3 and 4. These values are in good accord with the electron densities derived from other, smaller, samples such as in Stanghellini & Kaler (1989).

The diagrams provide direct and useful information on general physical conditions in PNe. For example, diluted shells with low electron density and low to moderate excitation conditions, e.g., $0.5 < \log [H\alpha/[\text{S II}]] < 1$ (see Fig. 5) will overlap the location of H II regions. These objects are likely large, evolved PNe. The likely presence of shock contributions in the dominantly photoionized environment of PNe is hinted at by objects located in Fig. 4 in the log $[H\alpha/[\text{N II}]] < 0$ and log $[H\alpha/[\text{S II}]] < 0.4$ region. Objects with high electron density and high $H\alpha$ emissivity in Figs. 5 and 6 point towards compact, young PNe. For PNe for which limited information is available, their location on the diagrams usually provides insight into their general (or peculiar) characteristics and evolutionary stage.

Figure 7 shows the histograms of the distribution of values for the corresponding line ratios. The numbers at the top of each bar indicate the percentage of objects in the sample associated with that value in relation to the entire sample. The line ratios of PNe are concentrated around a value of 1.2 for log $[H\alpha/[\text{S II}]]$ with a fairly even distribution on either side from the peak. For the log $[H\alpha/[\text{N II}]]$ line ratio the values concentrate around 0.0 but fall rapidly towards negative values. Finally, the distribution of values for the $[\text{S II}] \lambda\lambda6717/6731$ line ratio is markedly asymmetric, peaking sharply at a value of 0.6, with a smooth drop towards larger values and an abrupt fall on the other side (high density). These
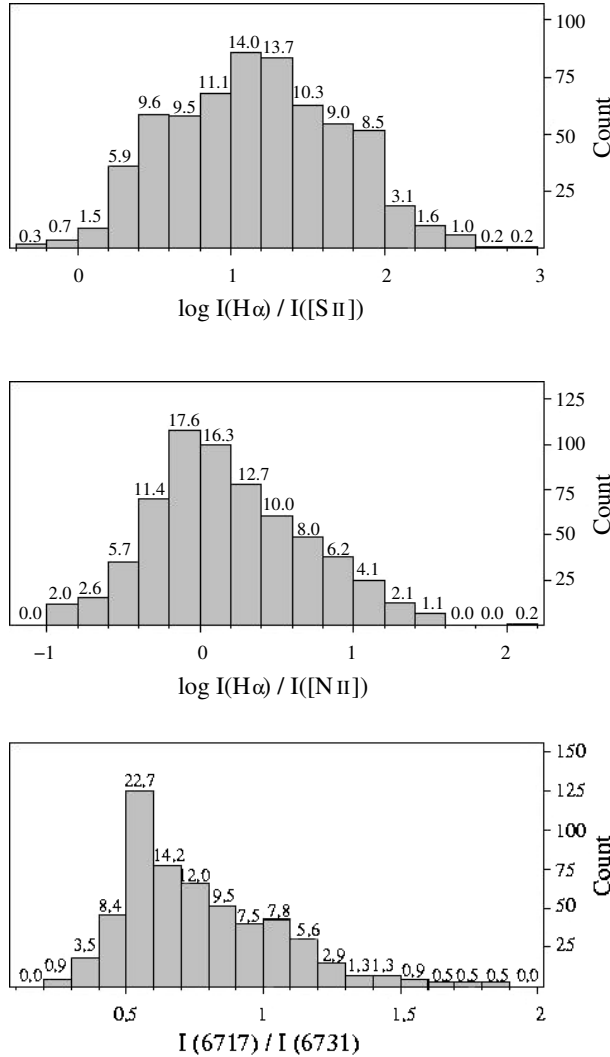

Fig. 7. Histograms of the distribution of the values for the corresponding line ratios. Numbers at the top of each bar correspond to the percentage value of that column in relation to the total sample.

with an 85% confidence level. The density ellipse is also a good graphical indicator of the correlation between the two variables involved. The ellipse collapses across its minor axis, i.e., becomes thinner, as the correlation between the two variables increases and approaches unity (± 1) and expands or reduces its eccentricity as the correlation weakens. The density ellipses in Figs. 4, 5, and 6 have all been set for a 0.85 probabilty; however the correlation coefficients differ among them, with values of 0.79, -0.58 and -0.37, respectively. Thus, the correlation between log $[H\alpha/[\text{S II}]]$ versus log $[H\alpha/[\text{N II}]]$ is strongest, whereas that between log $[H\alpha/[\text{N II}]]$ versus $[\text{S II}] \lambda\lambda6717/6731$ is weakest. The correlation is

values can be considered as representative for the most common or typical conditions in galactic PNe.

4. CONCLUSIONS

Values of $H\alpha/[N\,\textsc{ii}]$, $[S\,\textsc{ii}]$ $\lambda\lambda6717/6731$, and $H\alpha/[S\,\textsc{ii}]$ for 613 planetary nebulae have been derived from the Strasbourg Catalogue of Planetary Nebulae, part II (Acker et al. 1992) and plotted in the Sabbadin et al. (1977) diagnostics diagrams. The current sample substantially expands the sample used in the original diagrams and allows a redefinition of the parameter space of PNe in the log $[H\alpha/[S\,\textsc{ii}]]$ versus log $[H\alpha/[N\,\textsc{ii}]]$, log $[H\alpha/[S\,\textsc{ii}]]$ versus $[S\,\textsc{ii}]$ $\lambda\lambda6717/6731$, and log $[H\alpha/[N\,\textsc{ii}]]$ versus $[S\,\textsc{ii}]$ $\lambda\lambda6717/6731$ planes. Accordingly, new statistical limits have been set for the location of PNe in these diagrams using density ellipses of probability 0.85. We find a good, 0.79 correlation for the log $[H\alpha/[S\,\textsc{ii}]]$ versus log $[H\alpha/[N\,\textsc{ii}]]$ intensity ratio; a modest -0.58 correlation for the log $[H\alpha/[S\,\textsc{ii}]]$ versus log $[H\alpha/[N\,\textsc{ii}]]$ intensity ratio and a poor, -0.37 correlation in the case of log $[H\alpha/[N\,\textsc{ii}]]$ versus $[S\,\textsc{ii}]$ $\lambda\lambda6717/6731$. From our study we obtain the statistical distribution of emission line ratios expected in PNe. These upgraded diagnostic diagrams provide a better representation of the ranges of physical conditions indicated from the emission line ratios and allow the identification and study of groups or individual PNe of particular interest in specific regions of the diagrams.

Finally, in relation to the parameter space for the H II and SNR regions, the data sources in SMB77 for these two cases were restricted to a limited number of objects, as in the original case for PNe. For the H II regions the compilation made by Kaler (1976) was used. For the supernovae the data is based on 17 galactic remnants. It would be clearly useful to revise and update the parameter space for the H II and SNR regions so as to assess the reliability of their distributions in the revised diagrams. This is presently out of the scope of the present paper but worth pursuing as a natural extension of this work.

Templates in poscript or pdf format of the revised diagrams, Figs. 4, 5, and 6, are available from J. A. López.

REFERENCES

Acker, A., Ochsenbein, F., Stenholm, B., Tylenda, R., Marcout, J., & Schohn, C. 1992, Strasbourg-ESO Catalogue of Galactic Planetary Nebulae, ESO

Barral, J. F., Cantó, J., Meaburn, J., & Walsh, J. R. 1982, MNRAS, 199, 817

Daltabuit, E., D'Odorico, S., & Sabbadin, F. 1976, A&A, 52, 93

Dopita, M., A. 1976, ApJ, 209 395

García-Lario, P., Manchado, A., Riera, A., Mampaso, A., & Pottasch, S. 1991, A&A, 249, 223

Gutiérrez-Moreno, A., Moreno, H., & Cortés, G. 1995, PASP, 107, 462

Kaler, J. B. 1976, ApJS, 31, 517

López, J.A. & Meaburn, J. 1983, MNRAS, 204, 203

Osterbrock, D. E. 1974, Astrophysics of Gaseous Nebulae (San Francisco: W. H. Freeman and Co.)

Phillips, J. P. 2004, RevMexAA, 40, 193

Sabbadin, F., & D'Odorico, S. 1976, A&A, 49, 119

Sabbadin, F., Minello, S., & Bianchini, A. 1977, A&A, 60, 147

Stangehellini, L., & Kaler, J. B. 1989, ApJ, 343 811

Tajitsu, A., Tamura, S. Yadoumaru, Y., Weinberger, R., & Koppen, J. 1999, PASP, 111, 1157

José Alberto López and Hortensia Riesgo: Instituto de Astronomía, UNAM, Apdo. Postal 877, 22860 Ensenada, B. C., México (hriesgo@astrosen.unam.mx, jal@astrosen.unam.mx).